Biophysical Journal, Volume *116*

Supplemental Information

Magnetic Entropy as a Proposed Gating Mechanism for Magnetogenetic Ion Channels

Guillaume Duret, Sruthi Polali, Erin D. Anderson, A. Martin Bell, Constantine N. Tzouanas, Benjamin W. Avants, and Jacob T. Robinson

Supplementary Information: Magnetic entropy as a proposed gating mechanism for magnetogenetic ion channels

1 Magnetic Properties of Ferritin

As seen in Eq 2 in main text, magnetization of ferritin can be writen as:

$$M = M_0 \left[coth(\frac{\mu_p B}{kT}) - \frac{1}{\frac{\mu_p B}{kT}} \right] + \chi_1 B \tag{S1}$$

Here, μ_p is the magnetic moment for each ferrihydrite particle (1) ($\approx$ 345 μ_B, where μ_B is the Bohr Magneton). M_0 is the saturation magnetization, χ_1 is the susceptibility of the antiferromagnetic core. Both M_0 and χ_1 are temperature dependent. At 295 K, their values are $M_0 \approx 175$ Am^2 mol^{-1} and $\chi_1 \approx 56$ Am^2 mol^{-1} T^{-1} (using molecular weight of ferritin of 700 kDa (2)).

When the magnetic energy is small compared to the thermal energy ($\mu_p B << kT$), we can use the small angle approximation to write the Langevin function as $M = M_0 \frac{\mu_p B}{3kT}$, using the first term of its Taylor series expansion. At physiological temperature and magnetic field of 275 mT, the simplified form of the magnetization is accurate within 1%. Therefore, we have:

$$M = M_0 \left[\frac{\mu_p B}{3kT} \right] + \chi_1 B \tag{S2}$$

The values of $\left|\left(\frac{\partial M_0}{\partial T}\right)_B\right|$ and $\left|\left(\frac{\partial \chi_1}{\partial T}\right)_B\right|$ are obtained from the experimentally determined M_0 vs T and χ_1 vs T curves (1) to be 0.94 Am^2 mol^{-1} K^{-1} and 0.16 Am^2 mol^{-1} T^{-1} K^{-1} respectively.

2 Heat transfer between ferritin and ion channel

2.1 Calculation of g^*

We calculate the value of the thermal conductance scaling factor, g^* in the water shell model using temperature measurement data obtained from literature (3), (4), (5), (6), (7), (8). In all these experiments, iron oxide nanoparticles were heated using alternating magnetic fields. There are two different types of experiments: 1. Chemical measurements: In these experiments, thermolabile molecules are attached at different distances from the nanoparticle and the temperature is obtained by quantifying the amount of dissociated molecules collected after magnetic heating (3), (4) (Table S1 a-b). 2. Optical measurements: Direct real-time measurements were obtained using temperature dependent fluorescent/luminescent molecules attached to surface of nanoparticle (5), (6), (7), (8) (Table S1 c-g). We estimate a range of values for g^* for the different types of experiments using the following methods:

For the distance dependent chemical measurements, we use:

$$\Delta T_{NP} = \frac{W}{g^* G_{shell}} \tag{S3}$$

where ΔT_{NP} is the difference in temperature between the surface of the nanoparticle and the bulk. W is the power generated by the nanoparticle, G_{shell} is the thermal conductance due to a shell of water of radius r around the particle and is calculated as:

$$G_{shell} = -\frac{K_w}{\frac{1}{r_{NP}} - \frac{1}{r}} \tag{S4}$$

where K_w is the thermal conductivity of water (= 0.6 W m^{-1} K^{-1}) and r_{NP} is the radius of the nanoparticle. These distance dependent measurements have shown that temperature decays exponentially from the surface of the nanoparticle instead of the inverse-distance decay expected from Fourier law. Temperature decay constants obtained from these measurements are over 1 - 2 nm. Therefore, we assume a water shell of thickness 1.5 nm for calculating g^*. Also note that the temperature change at the surface of the nanoparticle (ΔT_{NP}) was obtained by the exponential fits to the distance dependent data. The estimated values of g^* for the chemical measurements is shown in Table S1 (a-b).

The increased thermal resistance around the particles causes a slow heat dissipation, thereby leaving the particle at a higher temperature for longer. Direct real time measurements show that temperature decay times are over a few 100 seconds for magnetically heated nanoparticles in suspension, after turning off the field. More recent experiment suggest decay times of 10 s for nanoparticles present on the surface of cell membrane (9). If $\tau_{d,NP}$ is the measured decay rate, g^* can then be estimated from $\tau_{d,NP}$ using:

$$\tau_{d,NP} = \frac{g^* G_{shell}}{C_s + C_{NP}} \tag{S5}$$

where G_{shell} is as described above, C_s is the heat capacity of the shell of water and C_{NP} that of the nanoparticle. C_s can be determined as:

$$C_s = C_{p,water} V_{shell} \rho_{water} \tag{S6}$$

where $C_{p,water}$ is the heat capacity of water (= 4185 J kg^{-1} K^{-1}), V_{shell} is the volume of the water shell of outer radius r and inner radius r_{NP}. ρ_{water} is the density of water (= 1000 kg m^{-3}). C_{NP} is evaluated using bulk magnetite heat capacity of 150 J mol^{-1} K^{-1} (10).

The estimated values of g^* for the direct real-time measurements is shown in Table S1 (c-g). The value of g^* obtained from the chemical measurements is higher and can be because the temperature data points used to estimate ΔT_{NP} are obtained outside the water shell.

Table S1: Calculation of g* based on experimental measurements of temperature near the surface of magnetically heated iron oxide nanoparticles

Distance dependent chemical measurements			
	g*	Decay constant (nm)	Reference
a	10^{-10}	2	Dias 2013
b	10^{-10}	1	Riedinger 2013
Real time optical measurements			
	g*	Decay rate constant (s^{-1})	Reference
c	$1.5x10^{-13}$	2×10^{-3}	Rinaldi 2012
d	3.5×10^{-13}	1.6×10^{-2}	Huang 2010
e	1.3×10^{-13}	4×10^{-3}	Piñol 2015
f	1.4×10^{-13}	5×10^{-3}	Dong 2014
g	2×10^{-12}	10^{-1}	Munshi 2017

a-f: Measurements from nanoparticles in suspension
g: Measurement from nanoparticles attached to cell membrane.

2.2 Calculation of c^*

As discussed in the main text, a specific domain of the protein could absorb the heat preferentially, before the channel reaches thermal equilibrium (**?**). To estimate the effect of this local heat absorption we can assume that a set of critical degrees of freedom (f^*) (e.g. a hydrogen bond) may absorb the energy and bias channel gating before the energy is equally distributed to all degrees of freedom (f) at thermal equilibrium. Thus we can define a heat capacity scaling factor $c^* = f^*/f$. Because temperature is a measure of the average kinetic energy in all degrees of freedom we can define an effective change in temperature for the critical degrees of freedom as $\Delta T^* = \frac{\Delta T}{c^*}$. Here, c^* is used to set bounds on the kinetic energy (or effective temperature) of any particular degree of freedom that might preferentially influence temperature-sensitive channel gating. In this case we see that c^* can vary between 1 (when heat is distributed between all degrees of freedom) and $1/f$ (when heat is absorbed by a single critial degree of freedom). Using the definition of heat capacity where $C_p = fk/2$ we can write the lower bound of c^* as $\frac{k}{2C_p}$. Based on the size of TRPV4 and the heat capacities of proteins of similar sizes (11), we estimate the value of channel heat capacity as 5×10^5 J mol^{-1} K^{-1}. Therefore, we have the range of values of c^* between 10^{-5} and 1.

2.3 Calculating channel temperature change

The temperature of the channel is estimated using the equivalent circuit in Fig 3b. In this equivalent circuit model, $\frac{dQ}{dt}$, T, C, and G, are replaced with current, voltage, capacitance, and conductance, respectively. We also assume that the water bath remains at a constant temperature (T_b). Heat transfer between the ferritin (f)/channel (c) and the near water shell (s) are assumed to be due to interfacial conductance. The interfacial conductances G_{fs} and G_{cs} are found to be $\approx 10^{16}$ W mol^{-1} K^{-1} based on the interfacial thermal conductance of 200 MW m^{-2} K^{-1} for protein-water (12) and AuPd nanoparticle-water interfaces (13) and assuming a 12 nm sphere for ferritin and a cube of side 12 nm for the channel. Conductance between ferritin and channel can be calculated using protein conductivity of 0.15 W m^{-1} K^{-1} and assuming a linker of 5 amino acids' length to get $G_{fc} \approx 10^{15}$ W mol^{-1} K^{-1}. G_{sb} is the conductance of the water shell and is the same as G_{shell} given in Eq. S4. In the case of lowered thermal conductances, (G_{sb}) will

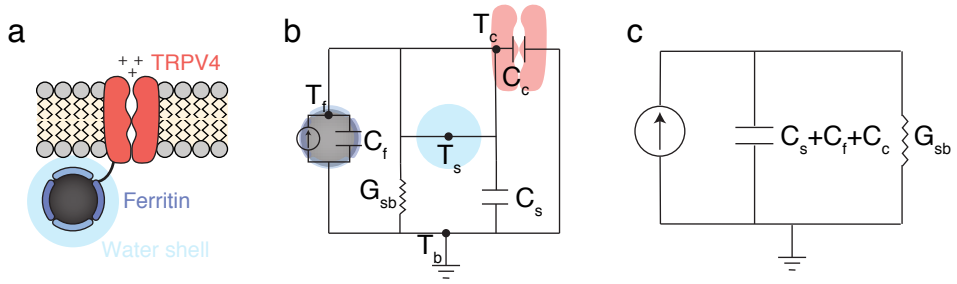

Fig. S1: a. Schematic for the water shell model: We propose that the thermal conductance of water surrounding the ferritin is lower than in macroscopic systems by a factor of g^*. (b) Simplified Equivalent circuit for the case where $G_{fs}, G_{cs}, G_{fc} \ll G_{sb}$. At this limit, G_{fs}, G_{cs}, G_{fc} in Fig. 3b can be replaced by short circuits. This circuit further simplifies to an RC circuit as in (c).

be multiplied by g^* resulting in $g^*G_{sb} \approx 2 \times 10^5$ W mol^{-1} K^{-1}. Because $G_{fs}, G_{cs}, G_{fc} \gg g^*G_{sb}$, we can assume that the ferritin, channel and water shell are all at the same temperature and simplify the equivalent circuit with G_{fs}, G_{cs} and G_{fc} shorted. The modified circuit is shown in Fig.S 1b. This circuit further simplifies to an RC circuit with $R = \frac{1}{g^*G_{sb}}$ and $C = C_s + C_c + C_f$ (Fig. S 1c). Based on bulk ferrihydrite heat capacity of 80 J mol^{-1} K^{-1} (14), we estimate heat capacity of ferritin (C_f) to be 10^5 J mol^{-1} K^{-1}. Based on the size of TRPV4 and the heat capacities of proteins of similar sizes (11), we estimate the value of channel heat capacity (C_c) as 5×10^5 J mol^{-1} K^{-1}.

To solve for temperature of the channel, ferritin and water shell, we write:

$$\frac{d\Delta T_c}{dt} = \frac{\frac{dQ_f}{dt} - g^*G_{sb}(T_c - T_b)}{C} \tag{S7}$$

Because we expect heat to dissipate much slower (over ≈ 10 s) compared to the magnetization time (1 s), we can assume all heat being provided at the same time (at $t = 0$) and thereby replace $\frac{dQ_f}{dt}$ with $Q_f\delta(t)$, where $\delta(t)$ is the Dirac Delta function in time and has unit of s^{-1}:

$$\frac{d\Delta T_c}{dt} = \frac{Q_f\delta(t) - g^*G_{sb}(T_c - T_b)}{C} \tag{S8}$$

The above differential equation can be solved easily to obtain:

$$\Delta T_c(t) = \frac{Q_f}{C} e^{-\frac{g^* G_{sb}}{C} t} \tag{S9}$$

The maximum temperature change therefore is governed by the ratio of heat generated and the heat capacities and is $\approx 2{\times}10^{-6}$ K for all values of g^*.

As mentioned earlier, the effective temperature seen by the channel might be greater due to temperature gradients resulting in specific degrees of freedom absorbing heat preferentially. Effective temperature change can be written as:

$$\Delta T_c^*(t) = \frac{Q_f}{c^* C} e^{-\frac{g^* G_{sb}}{C} t} \tag{S10}$$

Therefore, we have maximum effective channel temperature as a function of c^* (given by $\frac{Q_f}{c^* C} = \frac{2{\times}10^{-6}}{c^*}$). g^* governs the heat dissipation rate in the form of:

$$\tau_d = \frac{g^* G_{sb}}{C}. \tag{S11}$$

3 Calculating number of channel openings, m due to Magnetocaloric Effect

3.1 Magnetocaloric response in *Magneto2.0*

TRP channels are often modeled using a simple two-state open-close system. In this model, the temperature sensitivity of the channel is the result of temperature dependent changes in the opening rate (α) and the closing rate (β), which we can calculate from the Eyring equation (15):

$$\alpha = k_0 e^{\frac{\Delta S_{a,open}}{R}} e^{\frac{-E_{a,open}}{RT}}, \tag{S12}$$

$$\beta = k_0 e^{\frac{\Delta S_{a,close}}{R}} e^{\frac{-E_{a,close}}{RT}}, \tag{S13}$$

where $E_{a,open}$ and $E_{a,close}$ are the activation energies for channel opening and closing, respectively. $\Delta S_{a,open}$ and $\Delta S_{a,close}$ are the activation entropies for opening and closing. k_0 is the frequency factor given by $\frac{k_B T e^2}{h}$ with h being the Planck's constant. For a heat-gated channel, $E_{a,open} \ll E_{a,close}$ and so, α is much more sensitive to a temperature change than β. As a result, even a small increase in temperature leads to an increase in the number of channel openings. At steady state,

$$\frac{\alpha}{\beta} = \frac{P_{open}}{P_{close}} \tag{S14}$$

giving,

$$P_{open} = \frac{1}{1 + e^{\frac{(\Delta H_g - T\Delta S_g)}{RT}}} \tag{S15}$$

where $\Delta H_g = E_{a,open} - E_{a,close}$ is the gating enthalpy and $\Delta S_g = \Delta S_{a,open} - \Delta S_{a,close}$ is the gating entropy of the channel. Note that although the channel has a non-zero open probability at physiological temperatures, we expect the cell to adapt to maintain calcium homeostasis leading to no net calcium influx at steady state (16).

To compute the derivative of βP_{open} in Eq 8 (and thus the value of m) we use the expressions for β and P_{open} from Eq. S13 and Eq. S15 and the estimated values of the channel entropy and enthalpy change parameters: ΔH_g, ΔS_g, $E_{a,close}$, and $\Delta S_{a,close}$ for TRPV4. We can estimate the channel gating enthalpy, $\Delta H_g = 454$ kJ mol^{-1} and gating entropy, $\Delta S_g = 1496$ J mol^{-1} K^{-1}, by fitting published data for the P_{open} of TRPV4 expressed in HEK293 cells (17) to the closed form solution for P_{open} in Eq. S15. These fitted values of the activation parameters are of the same order of magnitude as those determined experimentally for TRPV1, for which $\Delta H_g = 208$ kJ mol^{-1} (15) and $\Delta S_g = 590$ J mol^{-1} K^{-1} (18). Although experimentally determined values for the channel activation enthalpy and entropy, $E_{a,close}$ and $\Delta S_{a,close}$ are unavailable for TRPV4, we can set bounds for these values

based on the limits for the channel response time of TRPV1, t_s (10^{-5} s $\leq t_s \leq$ 10^{-1} s) (15) which depends on the rates, α and β as follows:

$$t_s = \frac{1}{\alpha + \beta}. \tag{S16}$$

Substituting the expressions for α and β from (15) into this inequality yields:

$$10^1 \leq k_0 e^{\frac{\Delta S_{a,close}}{R}} e^{\frac{-E_{a,close}}{RT}} \left[1 + e^{\frac{-(\Delta H_g - T\Delta S_g)}{RT}}\right] \leq 10^5. \tag{S17}$$

For the above inequality to hold in TRPV4's operational temperature range of 20 - 45 °C, the range of allowable values for ($E_{a,close}$, $\Delta S_{a,close}$) should be within the triangular parameter space enclosed by the vertices (28 kJ mol^{-1}, -145 J mol^{-1} K^{-1}), (0, -242 J mol^{-1} K^{-1}), (0, -234 J mol^{-1} K^{-1}). Thus we can select any point within this parameter space to compute a value of m. Fortunately, all points within this parameter space yield comparable values for m. Selecting the most extreme values within this space causes m to vary by less than a factor of 2. For the purposes of estimating m, we assume a value of $E_{a,close}$ = 14 kJ mol^{-1} and $\Delta S_{a,close}$ = -192 J mol^{-1} K^{-1} which is approximately at the center of the parameter space such that the range of allowed m values are within a factor of 2. The experimentally determined value of E_{a_close} for TRPV1 is 23 kJ mol^{-1}, which is in the same ballpark. Correspondingly, the value of $E_{a,open}$ for TRPV4 is 440 kJ mol^{-1}, which is within a factor of two as that of TRPV1's 208 kJ mol^{-1}. As mentioned above, the huge difference between the values of $E_{a,open}$ and $E_{a,close}$ leads to the high temperature sensitivity of these channels. The calculated values of m are plotted in Fig. 3f.

Because β changes very slowly with temperature (15), one can further simplify the expression for m by making the approximation that $P_{open}\frac{d\beta}{dT} \ll \beta\frac{dP_{open}}{dT}$, and hence we can write:

$$\frac{d(\beta P_{open})}{dT} \approx \beta\frac{dP_{open}}{dT} \tag{S18}$$

This approximation is accurate to within 9%.

3.2 Magnetocaloric response in *MagM8*

Cold gated channels such as TRPM8 are also modeled using a two-state system. Since we are using the K856A mutant, the values of gating enthalpy and entropy are different from those for TRPM8 and given by: ΔH_g = -150 kJ mol^{-1}; ΔS_g = -520 J mol^{-1} K^{-1} (19). Although the opening and closing activation energies and entropies have not been determined experimentally, we constrained the values of the channel response time, t_s between 10^{-5} and 10^{-2} s within its operating temperature range of 10 - 40 °C ((15), (19)) and obtained a triangular parameter space enclosed by vertices ($E_{a,close}$, $\Delta S_{a,close}$) = (175 kJ mol^{-1}, 401 J mol^{-1} K^{-1}), (0, -150 J mol^{-1} K^{-1}), (0, -210 J mol^{-1} K^{-1}). For the purpose of calculating m, we take the parameter values from the first vertex because they are closest to the values for TRPM8 (15).

Fig. S2 shows values of m for a single magnetic stimulus obtained for *MagM8* using the above parameters for various values of c^* and g^*.

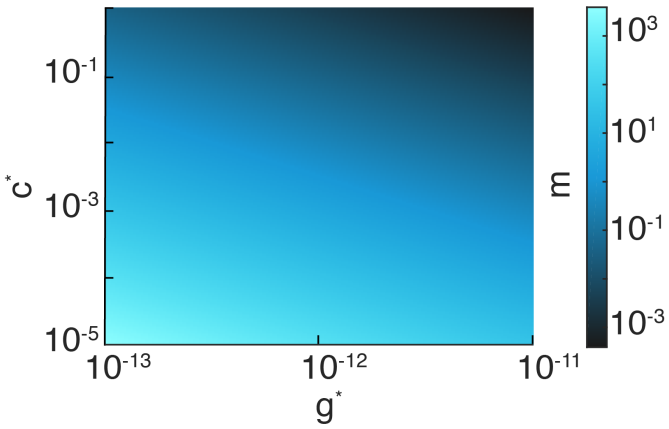

Fig. S2: Number of additional channel openings (m) due to magnetocaloric cooling of *MagM8* as function of c^* and g^*.

3.3 Magnetocaloric modulation of neural activity

We can calculate the current through a single TRPV4 channel using the following:

$$q = (E_{Ca^{2+}} - V_{m,neuron})g_{Ca^{2+}}, \tag{S19}$$

where $E_{Ca^{2+}}$ = 129 mV is the calcium reversal potential (20), $V_{m,neuron}$ = -70 mV is the resting membrane potential of a neuron, $g_{Ca^{2+}} \approx 60$ pS is the calcium conductance of TRPV4 (17). Using these values, we obtain an average current of 10 pA per channel at physiological temperature for an average open time of $t_{open} = 1/\beta = 5$ ms.

The minimum current amplitude of infinite duration that gives rise to an action potential in a neuron is called the rheobase and ranges between 15 - 900 pA (21), (22), (23). As the current level increases, the required pulse duration decreases. Chronaxie is the duration of a pulse required to generate an action potential in a neuron with a current of magnitude of twice the rheobase. Using these, we obtain the minimum required additional number of channel openings (m) for eliciting an action potential as:

$$m = \frac{2 \times \text{Rheobase/single channel current}}{\text{No. of channels per cell} \times \text{Probability}(t_{open} > \text{chronaxie})} \tag{S20}$$

The values of chronaxies range from 1 - 10 ms (24), and our average estimated open time (t_{open}) is well within this range. Using the fact that transfected hippocampal neurons can express between 160,000 and 1,000,000 heterologous functional TRPV1 channels (25), we find that values of m between 10^{-6} and 10^{-3} are sufficient to generate action potential in a neuron. These values fall well within the range of our theoretical predictions (Fig. 3f and Fig. S2) and could lead to action potentials or affect firing rates in the majority of transfected neurons.

3.4 Magnetocaloric effect on calcium concentration in HEK cells

Based on the fact that Fluo-4 (the indicator used for our experiments) can resolve a change of at least 85 nM (26) near the intracellular calcium concentration of 100 nM (20), we estimate that we can resolve a calcium influx of roughly 1.7×10^5 ions or greater in an HEK cell with a radius of 15 μm.

We can estimate that the average increase in the number of calcium ions in the cell, n, per channel opening is approximately 1.5×10^5 according to:

$$n = \frac{1}{2e}(E_{Ca^{2+}} - V_{m,HEK})g_{Ca^{2+}}t_{open}, \tag{S21}$$

where $E_{Ca^{2+}}$ = 129 mV is the calcium reversal potential (20), $V_{m,HEK}$ = -45 mV is the membrane potential of HEK cells (27), $g_{Ca^{2+}} \approx 60$ pS is the calcium conductance of the channel (17), e is the charge of a proton and t_{open} = 5 ms is the average open time of an activated channel (determined by $1/\beta$). Using these values, a single channel opening is near our expected limit for a detectable change in Fluo-4 fluorescence. We estimate approximately 1000 channels per HEK based on reported current densities for TRPV4 in HEKs (300 pA/pF at -100 mV, activated with agonist, 4αPDD (28)), and a single channel total conductance value of 60 pS (17), and an average capacitance of 20 pF for HEKs (as measured in our experiments). Therefore, m values on the order of 10^{-3} (which fall within the range of our theoretical predictions, Fig. 3f) would lead to a detectable increase in Ca^{2+} levels in each cell from a single magnetic stimulus. With repeated stimuli and the fact that not all cells need to respond for us to measure a magnetic response from the population, we expect that m values as small as 10^{-5} could explain our experimental results.

3.5 Effect of increasing frequency of stimulation

We use frequency of 0.08 Hz for stimulation in our experiments. Increasing the stimulation frequency is not expected to increase the number of channel openings (m) significantly. This is because the heat dissipation rate is estimated to be ≈ 0.1 s^{-1} (based on the equivalent circuit model in Fig. 3b and our assumed value of g^* obtained from published measurements of heat dissipation in magnetic nanoparticles (9)). Increasing the stimulation frequency above 0.1 Hz will cause the ferritin nanoparticles to be cooled by demagnetization before they can completely dissipate the heat generated by magnetization and thus higher stimulation frequencies are not expected to increase the response. Fig. S 3 plots the value of m as a function of frequencies upto 0.5 Hz.

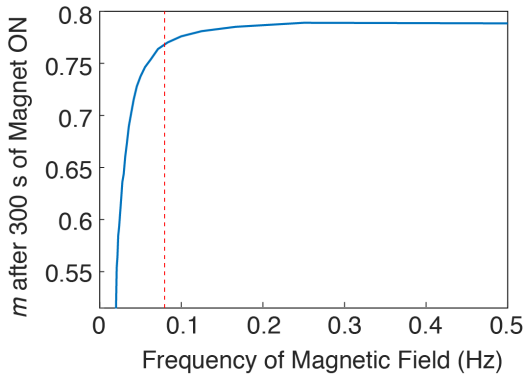

Fig. S3: Impact of stimulation frequency on channel openings: The total number of additional channel openings (m) at the end of a 300 s magnetic stimulation can be calculated for different stimulation frequencies. This calculation assumes $g^* = 2 \times 10^{-12}$ (corresponding to a heat dissipation rate of 0.1 s^{-1}) and $c^* = 10^{-5}$ (as in Fig. 3b) The value of m remains constant for frequencies ≥ 0.1 Hz. This value of g^* is obtained from the heat dissipation time of ≈ 10 s as measured by (9) from heated nanoparticles attached to the surface of cells.

Finally, at very large frequencies (> 100 Hz), the field switches faster than the non-linear responses of the cell (that result in higher calcium influx during magnetization than the net calcium efflux during demagnetization). In that case, the channel response is determined by the average channel temperature per cycle which decays based on the thermal relaxation rate of 0.1 s^{-1}. As seen in Fig. S 4, the temperature profile looks similar to that resulting from a single magnetization, irrespective of the duration of applied field. Since the average rise in temperature is half of that in the case of a single magnetization, the resulting m value would be half of that expected from applying a single magnetic stimulus.

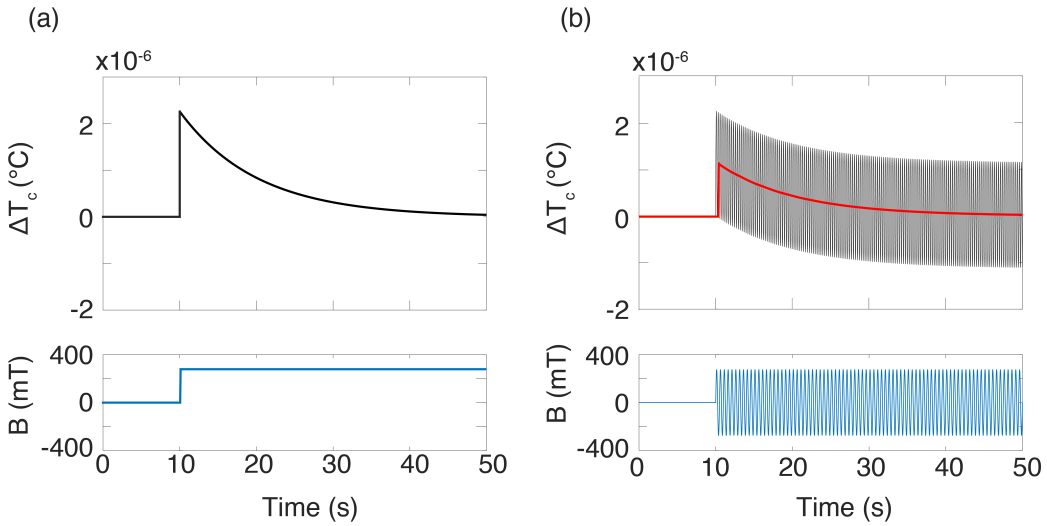

Fig. S4: (a) Change in channel temperature (ΔT_c) (top) due to magnetocaloric heating from a single magnetic stimulus (bottom). The temperature is raised by $\frac{Q_f}{C}$ and decays back to initial temperature at a rate determined by g^* (Eq S11 and Table 1). (b) Change in channel temperature (top) due to magnetocaloric effect in an RF magnetic field (bottom) modeled using Eq S7. The channel heats during magnetization and cools during demagnetization. The average temperature per cycle (red curve) decays at the same rate determined by g^*. Note also that the average rise in temperature is half of that in the case of a single magnetization. For clarity, we plot simulation with a 2 Hz magnetic field. We calculate that RF fields will generate a nearly identical temperature profile.

3.6 A note on thermal noise

Although TRP channels have a non-zero open probability at physiological temperatures, we expect the cell to adapt to maintain calcium homeostasis leading to no net calcium influx at steady state (16). The Maxwell-Boltzman temperature fluctuations of a single channel at room temperature is calculated to be 1.2 K using $\overline{\Delta T} = \sqrt{\frac{kT^2}{NC_c}}$ (29), where $N = 1$ for a single channel and C_c is its heat capacity ($\approx 5 \times 10^5$ J mol^{-1} K^{-1} from Section 2.3). But the cell is not sensitive to these fluctuations because its response is governed

by the ensemble average of the fluctuations of all of its channels. As the number of channels in a cell increases, the average temperature fluctuations of the ensemble decreases. Or in other words, the effect on the cell of a channel's positive deviation from average temperature is offset by that of another channel's negative deviation. Hence, although the increase in temperature caused by magnetocaloric heating is low, it causes a net increase in the number of channel openings at the cellular level.

For an ensemble of N channels in a cell, $\overline{\Delta T}$ is $1.2/\sqrt{N}$ K. These fluctuations are governed by atomic collisions that occur over a timescale of 10^{-14} s (20) while channel response times are in milliseconds. If we look at the sample average of these fluctuations at the millisecond timescale, we get:

$$\Delta T_{s.e.m} = \frac{\overline{\Delta T}}{\sqrt{t_{sam}/10^{-14}}} \tag{S22}$$

where t_{sam} is the sampling time and the sampling rate is 10^{-14} s. If we sample over 1 ms, we obtain 0.01 μK for $\Delta T_{s.e.m}$ of the ensemble of channels in a transfected neuron (with 160,000 channels (25)), which is much less than the minimum temperature change obtained from magnetocaloric effect (≈ 1 μK as seen in Eq. S9). It is therefore expected that the magnetocaloric-induced temperature changes have a significant physiological effect on the cell.

4 Supplemental Figures

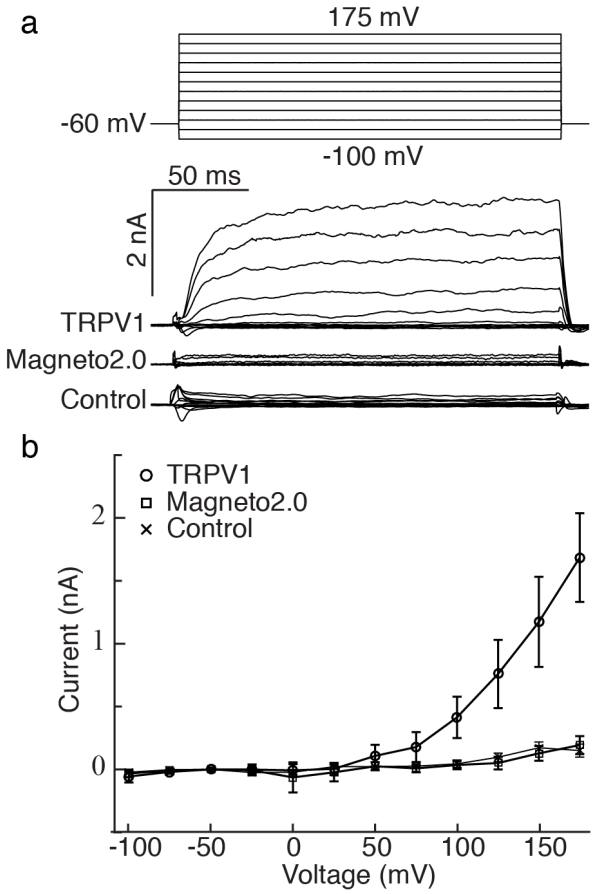

Fig. S5: Voltage sensitivity of *Magneto2.0*: (a) Representative whole cell patch clamp recordings obtained from HEK cells non transfected (control), or transfected with TRPV1 or *Magneto2.0*. (b) Average current from multiple cells for each condition ± s.d. n= 4, 5 and 6 independent cells for control, TRPV1 and *Magneto2.0* respectively. The absence of voltage sensitivity in *Magneto2.0* suggests that these channels would not be activated by eddy currents produced by dynamic magnetic fields (the activation mechanism for transcranial magnetic stimulation (TMS) (30)).

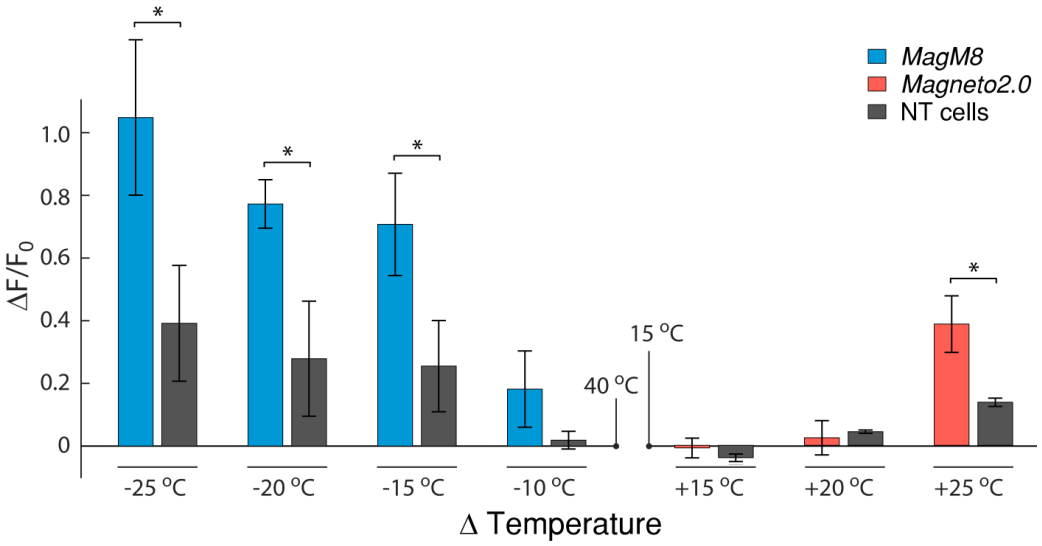

Fig. S6: Temperature responses of *Magneto2.0* and *MagM8*: HEK293 cells expressing *Magneto2.0* or *MagM8* were subjected to step changes in temperature while the intracellular calcium activity was monitored with Fluo-4. For cold stimulation, the temperature was stepped down to 30, 25, 20 and 15 °C from a starting temperature of 40 °C, and the response was recorded for cells expressing *MagM8* (blue bars) and non-transfected cells (grey bars). For heat stimulation, the temperature was stepped to 30, 35 and 40 °C from a temperature of 15 °C, and the calcium response was monitored for cells expressing *Magneto2.0* (red bars) and non-transfected cells (grey bars). The bars indicate the average maximum change in fluorescence measured after the temperature change, recorded from independent cell cultures (n = 3-5 slides per condition). The s.e.m. is computed using the number of slides for each condition. The significance is assessed with a two-tailed Students t-test (*: $p < 0.05$)

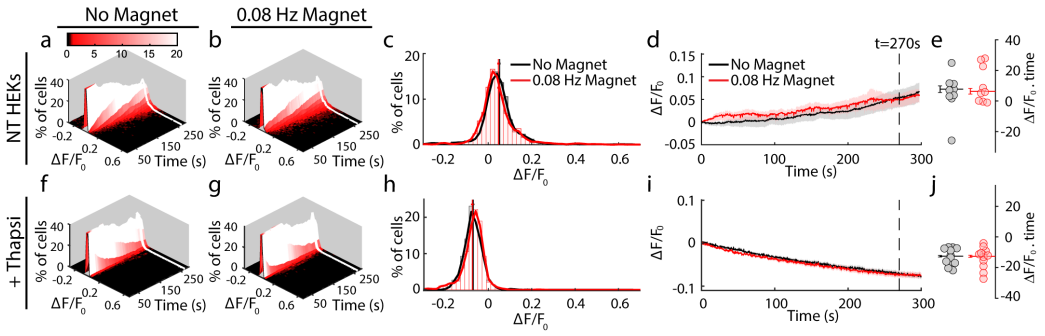

Fig. S7: Magnetic stimulation of non-transfected cells and calcium-store depleted cells: The intracellular calcium distribution is measured over time as the fluorescence of the calcium indicator Fluo-4, in (a-e) HEK293 cells non-transfected (NT), and (f-j) HEK293-*Magneto2.0* cells treated with thapsigargin (+Thapsi). (c) and (g): Histograms taken from the data in (a-b) and (f-g) respectively show the distribution of the fluorescence values at t = 270 s for all the cells recorded, with (red) or without (black) magnetic stimulation (bin size 0.02 $\Delta F/F$). Vertical red and black lines represent the mean value of these distributions and the error bars show the s.e.m. for each histogram (n > 800 cells). (d) and (i) $\Delta F/F_0$ values for each cell culture are averaged and plotted over time for stimulated (red) and non-stimulated (black) cells. The shaded regions show the s.e.m calculated using n = number of coverslips. The magnetic stimulation consists of 275 mT at 0.08 Hz, beginning at t = 30 s. For NT_{NoStim}: 1618 cells from 9 cell cultures, $\text{NT}_{MagStim}$: 1725 cells from 9 cell cultures. For Thapsi_{NoStim}: 812 cells for 12 cell cultures, $\text{Thapsi}_{MagStim}$ 825 cells for 12 cell cultures. Statistical significance for the average $\Delta F/F_0$ at 270 s. (c and h) and for the area under the fluorescence curve (e and j) was measured for values obtained for stimulated and non-stimulated populations, using a left tailed Wilcoxon; p > 0.5 for all.

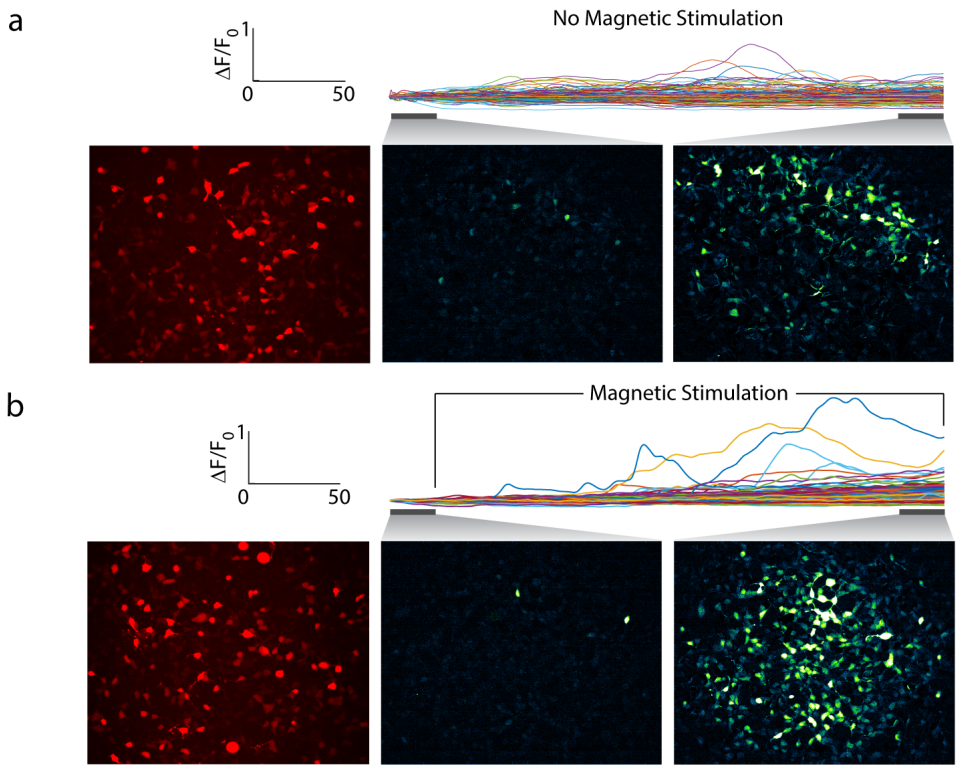

Fig. S8: Micrograph of cells transfected with *Magneto2.0*: These representative micrograph show the transfected cells (left panel), the Fluo-4 fluorescence intensity integrated for each pixel for the first 30 s of the recording (middle panel) and for the last 30 s of the recording (right panel). The traces above the micrographs show the fluoresence of Fluo-4 for each transfected cell.

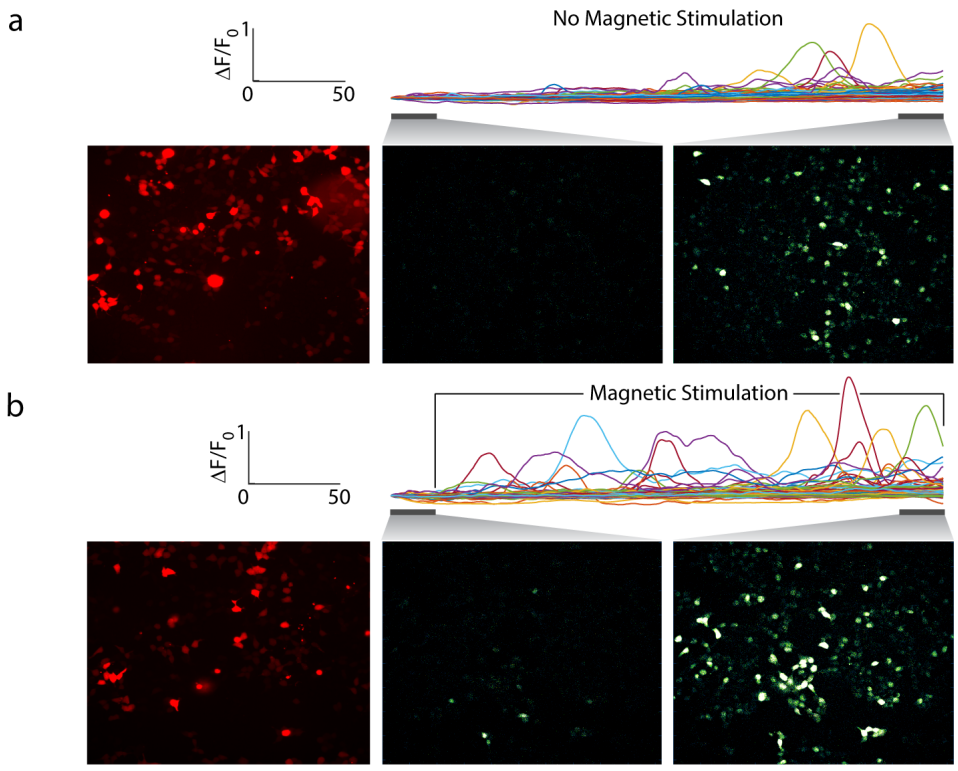

Fig. S9: Micrograph of cells transfected with *MagM8*: These representative micrograph show the transfected cells (left panel), the Fluo-4 fluorescence intensity integrated for each pixel for the first 30 s of the recording (middle panel) and for the last 30 s of the recording (right panel). The traces above the micrographs show the fluoresence of Fluo-4 for each transfected cell.

References

[1] S. a. Makhlouf, F. T. Parker, and a. E. Berkowitz, "Magnetic hysteresis anomalies in ferritin," Physical Review B, vol. 55, no. 22, pp. R14717–R14720, 1997.

[2] I. Fankuchen, "Ferritin: V. X-Ray diffraction data on ferritin and apoferritin," Journal of Biological Chemistry, vol. 150, pp. 57–60, 1943.

[3] J. T. Dias, M. Moros, P. Del Pino, S. Rivera, V. Grazú, and J. M. De

La Fuente, "DNA as a molecular local thermal probe for the analysis of magnetic hyperthermia," Angewandte Chemie - International Edition, vol. 52, no. 44, pp. 11526–11529, 2013.

[4] A. Riedinger, P. Guardia, A. Curcio, M. A. Garcia, R. Cingolani, L. Manna, and T. Pellegrino, "Subnanometer local temperature probing and remotely controlled drug release based on azo-functionalized iron oxide nanoparticles.," Nano letters, vol. 13, pp. 2399–406, jun 2013.

[5] H. Huang, S. Delikanli, H. Zeng, D. M. Ferkey, and A. Pralle, "Remote control of ion channels and neurons through magnetic-field heating of nanoparticles.," Nature nanotechnology, vol. 5, no. 8, pp. 602–606, 2010.

[6] R. Piñol, C. D. S. Brites, R. Bustamante, A. Martínez, N. J. O. Silva, J. L. Murillo, R. Cases, J. Carrey, C. Estepa, C. Sosa, F. Palacio, L. D. Carlos, and A. Millán, "Joining time-resolved thermometry and magnetic-induced heating in a single nanoparticle unveils intriguing thermal properties.," ACS nano, vol. 9, pp. 3134–42, mar 2015.

[7] J. Dong and J. I. Zink, "Taking the temperature of the interiors of magnetically heated nanoparticles.," ACS nano, vol. 8, pp. 5199–207, may 2014.

[8] L. Polo-Corrales and C. Rinaldi, "Monitoring iron oxide nanoparticle surface temperature in an alternating magnetic field using thermoresponsive fluorescent polymers," Journal of Applied Physics, vol. 111, no. 7, 2012.

[9] R. Munshi, S. M. Qadri, Q. Zhang, I. Castellanos Rubio, P. del Pino, and A. Pralle, "Magneto-thermal genetic deep brain stimulation of motor behaviors in awake, freely moving mice," eLife, vol. 6, aug 2017.

[10] M. Chase, NIST-JANAF Thermochemical Tables 2 Volume-Set (Journal of Physical and Chemical Reference Data Monographs). American Institute of Physics, fourth edition ed., 1998.

[11] J. Gomez, V. J. Hilser, D. Xie, and E. Freire, "The heat capacity of proteins," Proteins: Structure, Function, and Bioinformatics, vol. 22, no. 4, pp. 404–412, 1995.

[12] A. Lervik, F. Bresme, S. Kjelstrup, D. Bedeaux, and J. Miguel Rubi,

"Heat transfer in proteinwater interfaces," Physical Chemistry Chemical Physics, vol. 12, no. 7, p. 1610, 2010.

[13] Z. Ge, D. G. Cahill, and P. V. Braun, "AuPd metal nanoparticles as probes of nanoscale thermal transport in aqueous solution," Journal of Physical Chemistry B, vol. 108, no. 49, pp. 18870–18875, 2004.

[14] C. Snow, K. Lilova, A. Radha, Q. Shi, S. Smith, A. Navrotsky, J. Boerio-Goates, and B. Woodfield, "Heat capacity and thermodynamics of a synthetic two-line ferrihydrite, FeOOH·0.027H2O," The Journal of Chemical Thermodynamics, vol. 58, pp. 307–314, mar 2013.

[15] T. Voets, G. Droogmans, U. Wissenbach, A. Janssens, V. Flockerzi, and B. Nilius, "The principle of temperature-dependent gating in cold- and heat-sensitive TRP channels.," Nature, vol. 430, no. 7001, pp. 748–754, 2004.

[16] T. Wang, H. Xu, J. Oberwinkler, Y. Gu, R. C. Hardie, and C. Montell, "Light activation, adaptation, and cell survival functions of the Na +/Ca2+ exchanger CalX," Neuron, vol. 45, no. 3, pp. 367–378, 2005.

[17] H. Watanabe, J. Vriens, S. H. Suh, C. D. Benham, G. Droogmans, and B. Nilius, "Heat-evoked activation of TRPV4 channels in a HEK293 cell expression system and in native mouse aorta endothelial cells," Journal of Biological Chemistry, vol. 277, no. 49, pp. 47044–47051, 2002.

[18] J. Vriens, B. Nilius, and T. Voets, "Peripheral thermosensation in mammals," Nat Rev Neurosci, vol. 15, pp. 573–589, sep 2014.

[19] T. Voets, G. Owsianik, A. Janssens, K. Talavera, and B. Nilius, "TRPM8 voltage sensor mutants reveal a mechanism for integrating thermal and chemical stimuli," Nature Chemical Biology, vol. 3, pp. 174–182, mar 2007.

[20] B. Hille, Ion Channels of Excitable Membranes. Sinauer Associates, third edition ed., 2001.

[21] B. E. McKay and R. W. Turner, "Physiological and morphological development of the rat cerebellar Purkinje cell," The Journal of Physiology, vol. 567, pp. 829–850, sep 2005.

[22] A. Szücs, F. Berton, P. P. Sanna, and W. Francesconi, "Excitability of jcBNST Neurons Is Reduced in Alcohol-Dependent Animals during

Protracted Alcohol Withdrawal," PLoS ONE, vol. 7, p. e42313, aug 2012.

[23] N. Z. Gungor, R. Yamamoto, and D. Pare, "Optogenetic study of the projections from the bed nucleus of the stria terminalis to the central amygdala," Journal of Neurophysiology, vol. 114, pp. 2903–11, nov 2015.

[24] D. Brocker and W. Grill, "Principles of electrical stimulation of neural tissue," Handbook of Clinical Neurology, vol. 116, pp. 3–18, 2013.

[25] B. V. Zemelman, N. Nesnas, G. A. Lee, and G. Miesenbock, "Photochemical gating of heterologous ion channels: Remote control over genetically designated populations of neurons," Proceedings of the National Academy of Sciences, vol. 100, no. 3, pp. 1352–1357, 2003.

[26] I. D. Johnson and M. T. Spence, Molecular Probes Handbook: A Guide to Fluorescent Probes and Labeling Technologies. Life Technologies Corporation, 2010.

[27] R. Fliegert, G. Glassmeier, F. Schmid, K. Cornils, S. Genisyuerek, A. Harneit, J. R. Schwarz, and A. H. Guse, "Modulation of Ca2+ entry and plasma membrane potential by human TRPM4b," FEBS Journal, vol. 274, no. 3, pp. 704–713, 2007.

[28] T. Voets, J. Prenen, J. Vriens, H. Watanabe, A. Janssens, U. Wissenbach, M. Bödding, G. Droogmans, and B. Nilius, "Molecular determinants of permeation through the cation channel TRPV4," Journal of Biological Chemistry, vol. 277, no. 37, pp. 33704–33710, 2002.

[29] Y. Mishin, "Thermodynamic theory of equilibrium fluctuations," Annals of Physics, vol. 363, pp. 48–97, 2015.

[30] J. Banerjee, M. E. Sorrell, P. A. Celnik, and G. Pelled, "Immediate Effects of Repetitive Magnetic Stimulation on Single Cortical Pyramidal Neurons," PLOS ONE, vol. 12, p. e0170528, jan 2017.